PCCP

Accepted Manuscript

Journal Name

Dynamic Article Links ▶

ARTICLE TYPE

Self-Assembly of Long Chain Fatty Acids: Effect of Methyl Branch

Jonathan F. D. Liljeblad,[a] Eric Tyrode,[a] Esben Thormann,[a,b] Ann-Claude Dublanchet,[c] Gustavo Luengo,[c] C. Magnus Johnson[a] and Mark W. Rutland[a,d*]

The morphology and molecular conformation of Langmuir-Blodgett deposited and floating monolayers of a selection of straight chain (eicosanoic acid, EA), iso (19-methyl eicosanoic acid, 19-MEA), and anteiso (18-methyl eicosanoic acid, 18-MEA) fatty acids have been investigated by Vibrational Sum Frequency Spectroscopy (VSFS), AFM imaging, and the Langmuir trough. While the straight chain fatty acid forms
10 smooth, featureless, monolayers, all the branched chain fatty acids display 10 – 50 nm size domains (larger for 19-MEA than the 18-MEA) with a homogeneous size distribution. A model is suggested to explain the domain formation and size in terms of the branched fatty acid packing properties and the formation of hemispherical caps at the liquid-air interface. No difference between the chiral (S) form and the racemic mixture of the 18-MEA is observed with any of the utilized techniques. The aliphatic chains of the
15 straight chain fatty acids appear to be oriented perpendicular to the sample surface, based on an orientational analysis of VSFS data and the odd / even effect. In addition, the selection of the subphase (neat water or $CdCl_2$ containing water buffered to pH 6.0) used for the LB-deposition has a profound influence on the monolayer morphology, packing density, compressibility, and conformational order. Finally, the orientation of the 19-MEA dimethyl moiety is estimated, and a strategy for performing an orientational
20 analysis to determine the complete molecular orientation of the aliphatic chains of 19-MEA and 18-MEA is outlined and discussed.

[a] School of Chemistry, Division of Surface and Corrosion Science, KTH Royal Institute of Technology, SE-100 44 Stockholm, Sweden
25 _[b] Current address: Department of Chemistry, Technical University of Denmark, Kemitorvet 207, DK-2800 Kgs. Lyngby, Denmark_
[c] L'Oréal Research and Innovation, Aulnay-sous-Bois, France
[d] SP Technical Research Institute of Sweden, Chemistry, Materials and Surfaces, Box 5607, SE-114 86 Stockholm, Sweden
30 _* Correspondence: mark@kth.se, Telephone: +4687909914_
† Electronic Supplementary Information (ESI) available: 1. Additional AFM images of the branched chain fatty acid monolayers. 2. Orientational analysis of the 19-MEA dimethyl moiety. 3. Discussion on the curvature of the MEA and the possibility of spherical cap shaped
35 micelles. 4. Fitting parameters. See DOI: 10.1039/b000000x/

1. Introduction

Iso- and anteiso fatty acids are monomethyl branched chain fatty acids with their additional methyl group located at the ω-1 or ω-2 position respectively.[1] Although present in considerably smaller
40 amounts than their straight chain analogues, they play an essential role in biological systems.[2, 3]

One of the most investigated anteiso fatty acids is without doubt the (S)-18-methyl-eicosanoic acid which is covalently bound via an ester or thioester linkage to the surface of human hair. It con-
45 stitutes approximately 60% of the fatty acid mixture covering the surface of hair, and is found on the fur of almost all mammals.[2, 4] Because of this 18-MEA is assumed to have a profound influence on the surface properties of human hair, and it is thus of great interest in dermatology and cosmetology.[4] The reasons for the
50 enrichment of 18-MEA on the hair surface are poorly understood. The main differences compared to corresponding straight chain fatty acids appears to be the lower melting temperature without the inherent oxidation instability which double bonds would engender,[2, 5, 6] together with the different packing structure due to
55 the space requirements of the methyl branch.[1] In addition, the inhibition of bilayer formation and a better match of the area per molecule to the limited number of cysteine residues available for anchoring the fatty acids to the macromolecular structure have been proposed.[2] Furthermore shorter chain anteiso fatty acids
60 have proven to possess bacteriostatic properties[1, 7] and because various iso and anteiso fatty acids are commonly found in bacteria they are even used as taxonomic indicators.[3, 8]

Both floating and deposited mono- and multilayers of straight chain saturated and unsaturated fatty acids have been extensively
65 investigated by a wide variety of techniques such as X-rays, AFM, LB-experiments, and spectroscopic techniques[9-11]. The number of studies related to the molecular conformation and other monolayer properties of iso and anteiso fatty acids are,

however, scarcer. Previous investigations encompass for instance ATR-FTIR measurements and compression isotherms of 18- and 19-MEA,[12] compression isotherms of iso fatty acids of various chain lengths,[13] molecular dynamics simulation of 18-MEA,[14, 15] and tribological measurements.[16, 17] In addition, the influence on the structural and adhesive properties of human hair due to the replacement of 18-MEA by straight chain analogues in the Maple Syrup Urine Disease (MSUD) syndrome have been investigated.[2] In particular, to the best of our knowledge, no systematic comparison of the properties of the racemic mixture and the chiral (S) enantiomer of 18-MEA has been performed. This would be of particular interest since the racemic mixture is easier to synthesize[18] and is commonly used as a model system for the outer surface of hair, despite the latter only containing the (S) enantiomer. An important aspect that is often overlooked in the study of deposited monolayers is their assessment by an imaging technique such as AFM to ensure that the deposited film is indeed a homogeneous monolayer and does not possess structural features which may lead to misinterpretations in analysis of X-ray or spectroscopic data.

In this study we aim to increase the understanding of the influence of the methyl branch on the molecular packing and orientation by investigating LB-deposited monolayers of eicosanoic acid, 19-Methyl eicosanoic acid, and both the chiral (S) form and the racemic mixture of 18-Methyl eicosanoic acid by combining Vibrational Sum Frequency Spectroscopy (VSFS) with AFM imaging and the Langmuir trough. The trough has proven to be a valuable tool for investigating the macroscopic physicochemical properties of floating monolayers in the absence of the influence of a substrate. In addition it can be used to deposit these monolayers on solid substrates to enable investigations with other techniques, such as Atomic Force Microscopy (AFM) - to provide images at nm resolution, as well as force and friction measurements - or VSFS.[19-21] The latter is an inherently surface specific spectroscopic technique with sub-monolayer sensitivity. In contrast to AFM, VSFS is highly sensitive to conformational order and further enables determination of the orientation of molecular species. These properties render it a useful tool for investigating deposited[22, 23] or floating monolayers[24, 25] as well as other types of interfacial films.[26, 27] The three techniques provide complementary information and their combination is essential to enable full comprehension of the data generated by the individual techniques alone. In particular the combination of VSFS with AFM is essential, since the images can be used to verify the integrity, and confirm the common assumption of the homogeneity, of the investigated monolayer upon which the data analysis relies, thus increasing the validity of the results from the spectroscopic techniques.

2. Experimental Section

2.1 Materials

The (S)-18-methyl-eicosanoic acid ((S)-18-MEA) was custom synthesized by Larodan Fine Chemicals AB (Malmo, Sweden) based on a previously described procedure[18] modified by using chiral starting material. The rac-18-methyl-eicosanoic acid (rac-18-MEA) was supplied by L'Oréal Research and Innovation (Aulnay-sous-Bois, France), and the rac-18-methyl-D3-

eicosanoic acid (rac-18-D3-MEA) was supplied by Qmx Laboratories (Essex, UK). Eicosanoic acid (EA) and nonadecanoic acid (NoA) were obtained from Sigma-Aldrich and the octadecanoic-D35 acid (OA-D35) was obtained from Larodan Fine Chemicals AB (Malmo, Sweden). Rac-19-methyl-eicosanoic acid (rac-19-MEA) was obtained from Sigma Aldrich. The structures of some of the fatty acids are shown in Figure 1. For preparation of fatty acid solutions chloroform, (VWR Prolabo AnalaR Normapur stabilized with 0.6 % of ethanol) was used as received. The ultra-polished IR-grade (Infrasil-302) silica cylinders, 0.25" x 0.5", 10/5 scratch/dig, Ra ≤ 0.5 nm used as substrates for the monolayers were obtained from Newport (Irvine, CA, USA). All water used was purified using a Millipore system featuring constant monitoring of the conductivity (> 18.2 MΩ·cm) and organic content (< 4 ppb). The silica substrates were cleaned by soaking in chromosulphuric acid followed by extensive rinsing and sonication in water. The 0.1 mM cadmium chloride ($CdCl_2$), pH 6.0, 0.1 mM carbonate buffer used as a subphase for LB-depositions was prepared using sodium hydrogen carbonate (Na-HCO_3),(Sigma-Aldrich), $CdCl_2$ (BDH Chemicals Ltd., Poole, United Kingdom), and hydrochloric acid (HCl) (Sigma Aldrich).
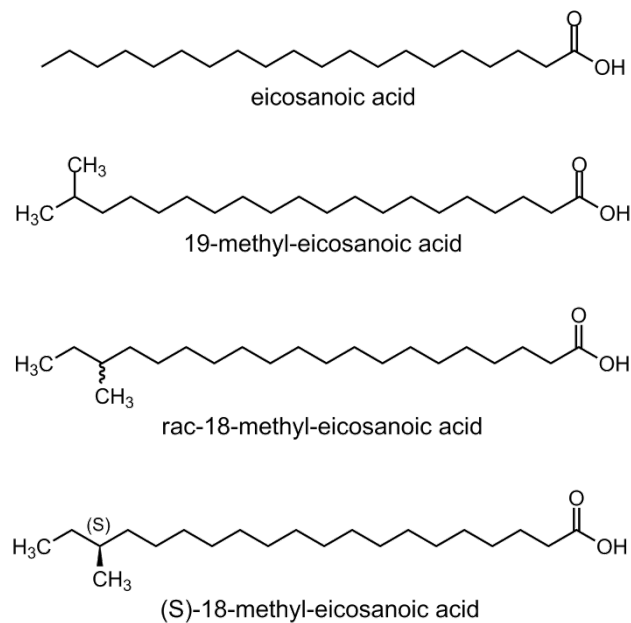
Figure 1. Molecular structures of a selection of the fatty acids studied.

2.2 Fatty acid Monolayer Preparation and Compression Isotherms

The preparation of the supported monolayers and the measurement of the compression isotherms were performed using a KSV 5000 LB system with the LayerBuilder software (KSV Instruments, Helsinki, Finland). The Teflon™ trough, 150 mm wide and with a useful area of 77 500 mm^2, featured hydrophilic polyoxymethylene (Delrin™) barriers, and was equipped with temperature control to maintain the subphase temperature at 20±0.2°C and a 10 mm wide paper plate as a probe for the surface pressure. All compression isotherms were recorded with a constant barrier speed of 5 mm/minute. The Langmuir-Blodgett deposition was performed by lifting the substrate vertically with a speed of 0.5 mm/minute while maintaining the surface pressure constant at the desired setpoint (20 mN/m unless otherwise stat-

ed). This pressure was chosen because it is below the collapse pressure of the 18-MEA and 19-MEA for a wide range of solution conditions.

The selection of the substrate used for supporting the deposited monolayers requires careful consideration. It has to be sufficiently smooth to enable AFM-imaging, insoluble in water, preferably transparent in the IR region, at least when probing the solid / liquid interface, and finally should not influence the investigated properties of the monolayer to any great extent. Mica sheets are atomically smooth without the need of any previous polishing, but suffer from strong absorption in the IR region that together with birefringence complicates spectroscopic investigations. Calcium fluoride is transparent in most of the IR range and fatty acids bind strongly to it.[28] However, it is slightly soluble in water and the released Ca^{2+} ions combined with the surface carbonation[29] may interact with the fatty acids and prevent the formation of a smooth monolayer.[30, 31] In addition it cannot be polished to achieve sufficiently low surface roughness. The ultra-polished fused IR grade silica used in this investigation represents a reasonable tradeoff since it is insoluble in water, sufficiently transparent in the IR range, and can be polished down to Ra < 0.5 nm. Furthermore, the deposition of fatty acid monolayers on silica has been extensively investigated.[9, 10]

2.3 VSF Spectrometer and data processing

The femtosecond VSF spectrometer used for this investigation is described in detail elsewhere[32] and only a brief description of its key features and principles is given here. Briefly, two high intensity pulsed laser beams, one with a fixed wavelength in the visible range and one tunable infrared (IR) are temporally and spatially overlapped at the sample surface. A third beam, with the sum frequency (SF) of the two incident beams is generated provided that the inversion symmetry is broken, which is of course the case at an interface. The SF signal is resonantly enhanced when the IR frequency overlaps with the vibrational frequencies of a molecule at the interface.

The laser source (Quantronix, USA.) consists of a Ti:Sapphire broadband oscillator creating an 800 nm seed pulse which is subsequently amplified in a combined regenerative and multipass system generating a 1 kHz train of 90 fs pulses centered at 806 nm with a total power of approximately 6.2 W. A tunable infrared pulse (1.14 μm -20 μm) is generated by a traveling wave optical parametric amplifier (He-TOPAS-C, Light Conversion, Lithuania) pumped with 75% of the laser power. The remaining power is used to create a bandwidth tunable picosecond pulse by a home built pulse shaper. The spectrometer features a high degree of automation and motorization to facilitate rapid data collection. A combined spectrometer and EM-CCD camera (Newton, Andor, Ireland) is used to collect the sum frequency signal. At normal operation typically a 4 mW IR beam focused to 0.15 mm and a 10 mW visible beam focused to 0.35 mm are used. The spectral resolution is < 4 cm⁻¹. The data presented in this investigation were recorded with the IR and visible angles of incidence set to 55° and 65° respectively in a copropagating geometry.

Due to the convolution of the spectral peaks with the Gaussian intensity distribution of the IR beam in the frequency domain a normalization procedure is required to restore the true shape and amplitude of the peaks.[32] This is performed by dividing the sample spectra by reference spectra obtained from gold using the same IR center frequencies and angles of incidence as used for recording the sample spectra. To avoid amplifying noise the low intensity wings are truncated, typically at ten percent of the maximum intensity, before the normalized spectra are added together to obtain the final spectra.

To extract the peak intensities and their relative phase the spectra were fitted with a sum of complex Lorentzian functions which allow for the constructive and destructive interference between adjacent bands and a real valued (since no absorption takes place in dielectrics) constant representing the non-resonant background (Equation (1)). Fitting was performed using the Levenberg-Marquardt algorithm in commercial software (Igor Pro version 6).

$$I_{SF}\left(\omega_{IR}\right) = \left| A_{NR} + \sum_n \frac{A_n}{\omega_n - \omega_{IR} - i\Gamma_n} \right|^2 \qquad (1)$$

In equation (1) A_{NR} denotes the non-resonant contribution to the SF signal, A_n is the amplitude of the n-th vibrational mode, ω_n and ω_{IR} represent the resonance frequency of the vibration and the infrared frequency respectively, and Γ_n is a constant accounting for the homogeneous broadening.

VSF spectra of the deposited fatty acids were recorded in the CH- and CD-stretching regions. All spectra were recorded at least three times and the presented data forms a representative selection. The absolute intensity of the spectroscopic signal depends on the precise overlap of the laser beams on the sample surface and the alignment of the sample in the spectrometer. Accordingly, only the intensities of the spectra presented in the same graph are directly comparable, unless otherwise stated, since they were recorded in the same experiment.

2.4 AFM

Topography and phase images of the deposited fatty acid monolayers were obtained using a Multimode Nanoscope V atomic force microscope (Bruker) operating in tapping mode. A high resolution silicon cantilever (DP15/Hi'Res-C, Mikromasch), with a nominal spring constant of 40 N/m, a resonance frequency of 325 kHz, and a high aspect ratio extra tip with a radius of approximately 1 nm, was used. For each sample, small scale images of 250 x 250 nm and large scale images of 1 x 1 μm or 5 x 5 μm were obtained at several different surface positions.

3. Results and Discussion

To further demonstrate the importance of combining different experimental techniques, the results from each of them are presented and interpreted separately. The subsequent concluding discussion draws conclusions only made possible by their combination.

3.1 Compression isotherms

The choice of subphase in the Langmuir trough has a profound influence on the floating monolayers as can be seen by comparing the pressure – area isotherms recorded on neat water (pH ≈ 5.6) and a pH 6.0 buffer containing Cd^{2+} ions (Figure 2a and b). The isotherms recorded on the neat water closely resemble literature data in terms of the lower compressibility (steeper slope) of

19-MEA compared to EA and 18-MEA, the slightly higher collapse pressure of 19-MEA compared to 18-MEA, and the phase change of the EA from a tilted to untilted condensed phase at approximately 26 mN/m.[12] A similar trend of increasing area per molecule when shifting a methyl branch from the end towards the middle position of the aliphatic chain has been observed both for stearic acid and phospholipids.[33]
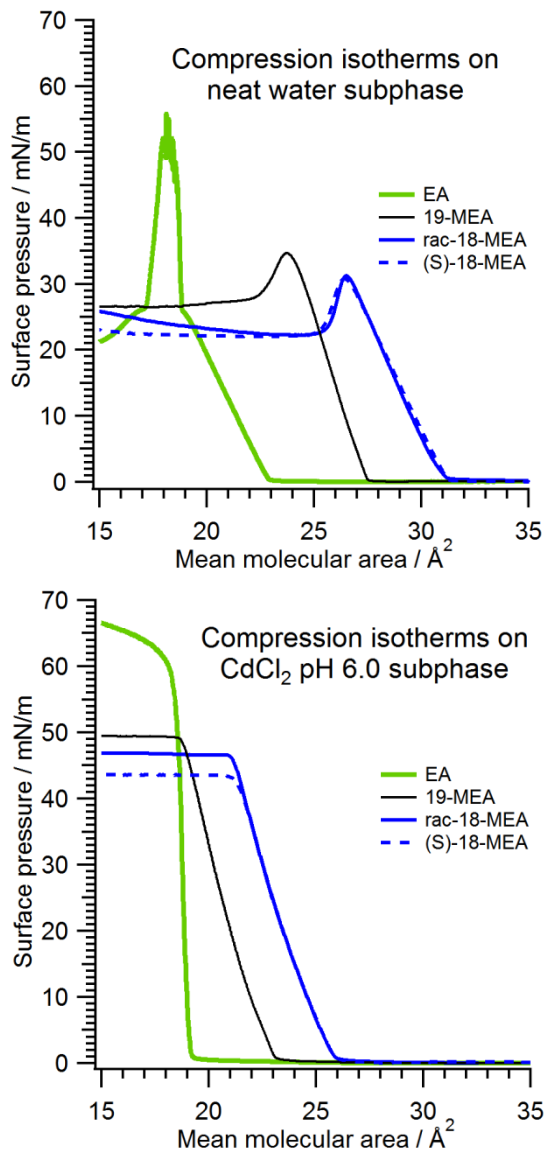
Figure 2A and B. Compression isotherms, of a selection of the investigated fatty acids, recorded on neat water (2A) and on CdCl₂, pH 6.0 carbonate buffer subphase (2B). Replacing the water subphase with the buffer results in a contraction of the monolayers, increases the collapse pressure, and shifts the collapse event from a *constant area* to a *constant pressure* type. The racemic and chiral 18-MEA isotherms have been arbitrarily shifted by ≈0.5 Å² each (within the error range) to overlay the curves and emphasize the fact that they are almost indistinguishable.

Replacing the neat water subphase with a 0.1 mM CdCl₂ subphase buffered to pH 6.0 strongly influences the shape of the isotherms. The tilted condensed phase of the EA vanishes, the areas per molecule of 19-MEA and 18-MEA decrease by approximately 5 Å² each, and the collapse pressure of all the fatty acid

monolayers increases. This well-known condensing and stabilizing effect on a fatty acid monolayer when adding divalent metal ions to the subphase is strongly pH dependent owing to the influence of the metal ions on the surface *pKa* of the fatty acids which in turn governs the formation of the metal salt.[10, 11, 34, 35]

Apart from the condensing effect by the Cd^{2+} ions the compressibility of the 19-MEA and 18-MEA are similar in the presence of the ions, which is not the case on the neat water subphase. To attempt to rationalize this finding, the mechanism of the influence of the divalent ions on the monolayers must be considered. The ions reduce the strength of the more long range headgroup repulsion, so that the shape of the isotherms is mainly governed by steric repulsion between the aliphatic chains, enabling a tighter packing.[10, 11, 36] This means that when tail interactions dominate, the compressibility of 18- and 19-MEA are identical, but when the interaction is dominated by headgroup repulsions in the neat water case the compressibility of 19-MEA differs from both the EA and the 18-MEA. Since the location of the methylation on the tail is the only difference, it is thus surprising that the compressibility is only different under conditions when the tails are expected to influence it the least. This could indicate that in the presence of stronger headgroup repulsion the tails adopt different conformations depending on the location of the methylation. The detailed mechanism of this influence on the compressibility however requires further investigations. A possible resolution of this apparent conflict is advanced in section 3.6 of the discussion. There it is argued that the presence of 3 dimensional, hemispherical cap shaped micelles at the liquid-air interface is consistent with the observations in this work.

Molecular dynamics studies have been performed to investigate the structure of Langmuir monolayers of EA and 18-MEA on water.[14] The results showed that a fraction of the 18-MEA molecules were shifted along the length axis so that the bulky ends of the aliphatic chains were expelled from the monolayer, leading to a displacement of the carboxylate group and thus placing the associated hydrating water in close contact with adjacent aliphatic chains. The selected areas per molecule used for *both* EA and 18-MEA in the simulations (24.5 Å² - 18.5 Å²) agree with the measured compression isotherm for EA but are all significantly smaller than the measured collapse area (*i.e.* the minimum area per molecule at which a monolayer can exist) of 18-MEA, meaning that they are unphysical. Since the molecular dynamics model probably precludes a realistic collapse mechanism it may be that the observed longitudinal shift of the chains is an "artifact" of this constraint.

The isotherms show that the collapse behavior changes from a *constant area* to a *constant pressure* type when replacing the neat water with the Cd^{2+} containing subphase. The constant area collapse is typical for fatty acid monolayers where the headgroups are not fully dissociated, promoting rapid formation of multilayers as the collapse pressure is reached.[34, 37] The collapse behavior gradually shifts to a constant pressure type as the pH is increased and full dissociation of the monolayer occurs.

Finally it is interesting to note that the compression isotherms of the racemic mixture and pure (S) enantiomer of the 18-MEA are very similar. More precisely, the shapes of the isotherms and the area per molecule at a given surface pressure are identical. This indicates that the racemic mixture and the pure enantiomer pack

in a similar manner when forming a floating monolayer. This observation is consistent with the fact that the bulk melting temperatures (which reflect the intermolecular spacing and packing) of the chiral S-form and the racemic mixture of 18-MEA are
5 similar, indicating similarity in the crystalline packing geometry.

3.2 AFM Imaging

The AFM tapping mode topography and phase images of the monolayers deposited on the ultra-smooth (Ra < 0.5 nm) silica surfaces are displayed in Figures 3, 4, and 5. In several cases the
10 phase images provide a better contrast than the topographical images and in Figure 4 and Figure 5 we thus present both types of images. For each sample both small scale images of 200 x 200 nm and large scale images of 1 x 1 μm or 5 x 5 μm were obtained at different surface positions, to assess the homogeneity of the
15 films. A selection of these images is presented in Figures 3, 4, and 5 and additional images are presented in the Supporting information (Figures S1 and S2).
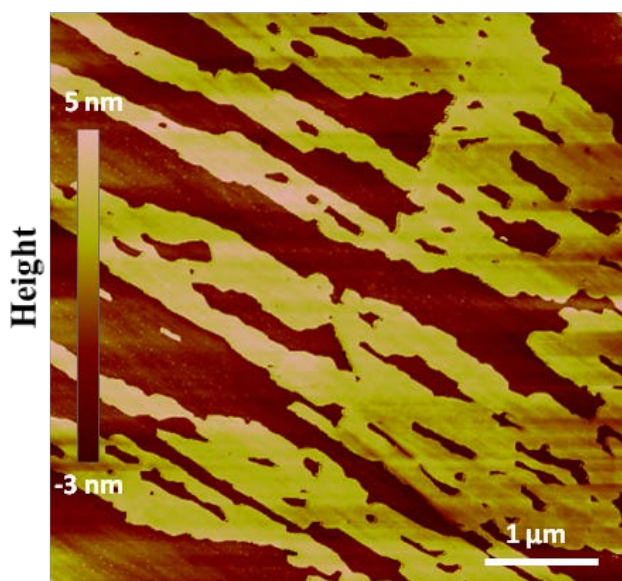
Figure 3. Topography AFM image of eicosanoic acid (EA) deposited on
20 silica from a neat water subphase. The 5 μm x 5 μm image, where the brighter parts are the fatty acid and the darker parts the bare silica surface, shows that the fatty acid monolayer only partly covers the silica surface. The thickness of the monolayer is approximately equal to the length of the molecules (2.4 nm).

25 Figure 3 shows a topography image of the monolayer deposited from a neat water subphase. Incomplete coverage is clearly seen in the 5 μm image. The roughness of the coated and uncoated regions is comparable, indicating that there are continuous monolayer regions, interspersed with bare patches. The height differ-
30 ence between the coated and uncoated regions is ≈2.5 nm as obtained from the peak to peak distance of the height distributions in the image and this value is consistent with the length of the molecule (2.4 nm). The relatively poor surface coverage ratio prompted the pursuit of different deposition conditions. In con-
35 trast, the images of EA deposited from the Cd^{2+} containing subphase show an almost complete coverage with only minor defects (Image S1 in the supporting information). The structure of this monolayer (Figure 4) is smooth with height variations of the order of one Ångström, reflecting the noise floor of the equipment.

40 The thickness of this monolayer is also approximately equivalent to the length of the molecules (2.4 nm) and no signs of bi- or multilayer formation were observed.

The transfer ratio (i.e. the loss of floating monolayer area during the deposition, divided by the covered substrate area) could con-
45 ceivably provide an additional indication of the degree of monolayer coverage on the substrate or if large structural changes occur during the deposition. This ratio relies; however, on the assumption that the area of the substrate is accurately known, and since a large proportion of the silica substrates are unpolished,
50 their effective area is difficult to estimate, rendering the transfer ratio at best a qualitative indicator. Because the AFM-imaging enables a much more detailed assessment of the coverage we refrain from reporting the transfer ratios.
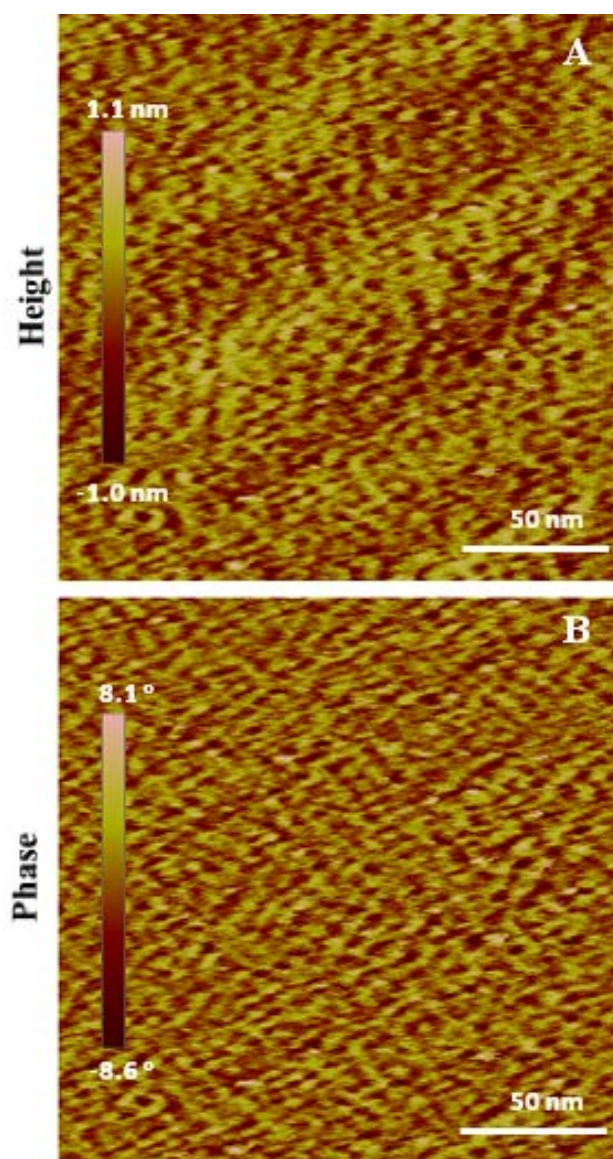
55 Figure 4A (top) and B (bottom). The topography and phase images of eicosanoic acid (EA) deposited on silica from a Cd^{2+} containing subphase reveal a smooth monolayer with an nm size pattern reflecting the noise floor of the equipment. In contrast to the EA deposited from the neat water subphase (Figure 3) this monolayer almost fully covers the surface.
60 (See Figure S1 in the Supporting information.)

The images of the racemic and chiral 18-MEA monolayers and 19-MEA monolayers presented in Figure 5A-C show a very different internal structure since there is unambiguous evidence for domain formation in all three samples. The shape and size (≈10 - 15 nm across) of the domains appear to be similar for the chiral and racemic 18-MEA and the images are essentially indistinguishable. The domains observed in the 19-MEA sample are

considerably larger (≈45 nm across) and the spacing between the domains is smaller. The domains display internal features, but they are certainly too large to be due to individual molecules: the sizes correspond rather to quite large clusters of molecules, since the distance between the individual aliphatic chains is expected to be of the order of 0.5 nm. The possible origin of the domains is discussed after the spectroscopic analysis in section 3.6.
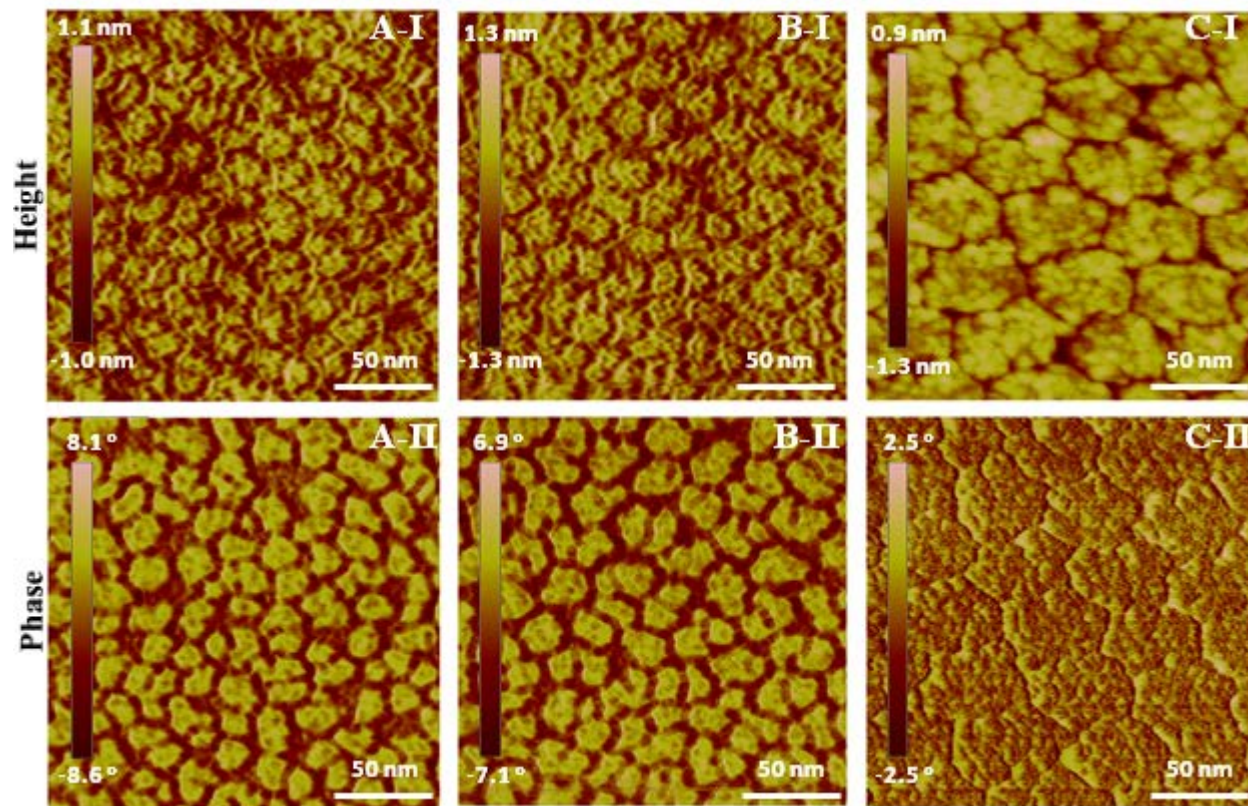
Figure 5A, B, and C. Topography and phase AFM images of A) rac-18-MEA, B) (S)-18-MEA, and C) 19-MEA deposited on silica from a Cd^{2+} containing subphase. In contrast to EA (Figure 4) all three fatty acids display domain formation. Both the chiral and racemic 18-MEA show identical 10 – 20 nm large domains while the 19-MEA displays larger domains. Additional images are presented in the Supporting information (Figure S2).

3.3 VSF Spectroscopy

3.3.1 Straight chain fatty acids
Subphase effects.

VSF spectroscopy provides information about the molecular structure of the sample, such as the conformational order, packing density, and the average tilt of the aliphatic chains. Comparing the spectra of the EA deposited from the neat water and Cd^{2+} containing subphase in Figure 6 and Figure 7A reveals profound differences in packing and conformational order of the two monolayers as will be discussed in detail below.

The sum frequency spectra of deposited monolayers of eicosanoic acid (EA) and nonadecanoic acid (NoA) shown in Figure 7A and B are almost identical. In the following section we show that the spectra indicate conformationally well-ordered and tightly packed aliphatic chains. Furthermore we demonstrate how to infer, both from orientational analysis based on the relative intensities of the peaks in different polarization combinations, and the odd / even effect, that the aliphatic chains are oriented approximately perpendicularly to the surface plane.

The assignment of the CH-stretching region is well established.[38-41] The spectra in Figure 7 are dominated by three peaks, namely

the symmetric methyl stretch, r^+, located at 2878 cm^{-1}, its Fermi resonance, r^+_{FR} at 2940 cm^{-1}, with an overtone of the methyl bending mode, and the antisymmetric methyl stretch, r^-, at 2965 cm^{-1}, which interferes destructively with the r^+_{FR} in SSP. The r^+_{FR} peak is strongest in SSP but also seems to appear as a small peak in PPP where it is less commonly resolved.[6] The symmetric methylene stretch, d^+, at 2845 cm^{-1} is almost absent in the spectra, and only gives a small contribution to the SSP combination. Finally, the antisymmetric methylene stretch (d^-) partly contributes to the broad feature around 2900 cm^{-1} in PPP. The ratio of the d^+ to r^+ intensities in SSP serves as an indicator of conformational order for protiated aliphatic chains since the d^+ intensity is very sensitive to *gauche* defects.[19, 42] In a tightly packed monolayer the chains are stretched to an all-*trans* conformation that does not generate any methylene signal because the methylene modes are intramolecularly coupled in an in phase and out of phase vibration which are not simultaneously IR and Raman active.[43] In the presence of gauche defects this coupling is disturbed and the methylene signals start to appear in the spectrum. However, since a completely isotropic surface film would not give rise to any VSF signal, an increasing disorder is also accompanied by a de-

creasing overall spectral intensity. Finally, it is worth noting that both constructive and destructive interference between the d⁺ mode and the r⁺ mode can be observed. The type of interference is most probably governed by the dominating orientation of the ⁵gauche defects and their location in the aliphatic chains in the monolayer. This represents an interesting topic of research to further expand the understanding of conformational indicators in aliphatic chains.[44]
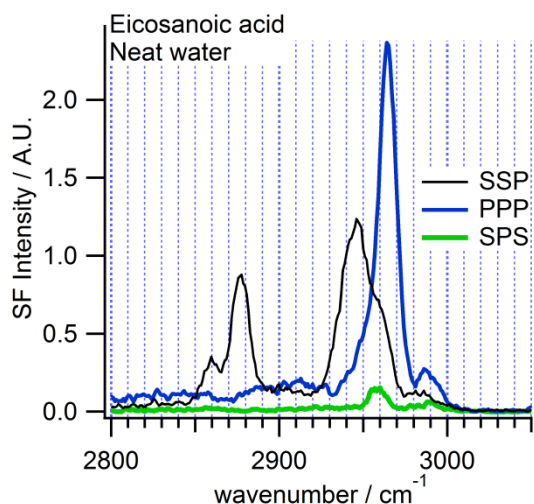
₁₀ Figure 6. VSF spectra of eicosanoic acid (EA) deposited on silica from a neat water subphase. Note that the antisymmetric methyl stretch is split in an in plane and out of plane component at ≈2960 cm⁻¹ and ≈2980 cm⁻¹ respectively (Compare Figure 7A). The spectra in this figure were obtained using a picosecond VSF spectrometer described elsewhere.[27]

₁₅ The spectra of the EA deposited on silica from a neat water subphase (Figure 6) differs from the corresponding spectra of EA deposited from a Cd²⁺ containing subphase shown in Figure 7A in terms of the splitting of the degenerate r⁻ mode into an in plane (at ≈2960 cm⁻¹) and out of plane (at ≈2980 cm⁻¹) component,[45, 46] ₂₀ and in addition a stronger contribution from the d⁺ mode is observed. This indicates a substantially different packing of this monolayer compared to the EA deposited from the Cd²⁺ containing subphase. Provided that the common assumption of free rotation of the methyl group around the C-C bond axis is valid it ₂₅possesses C_{3v} symmetry, but if the rotation is obstructed due to steric interactions with neighboring molecules, as is the case in a crystalline phase, the symmetry changes to C_s. In the latter symmetry the r⁻ vibration is split into an in plane and out of plane component, but when free rotation prevails they are merged into a ₃₀single degenerate mode. Non-degenerate methyl antisymmetric stretches have been observed in bulk long chain alkanes at room temperature and below using IR spectroscopy[45] but are only rarely seen with VSFS, for instance in zinc arachidate monolayers deposited on sapphire and in dodecanol at the air/liquid inter- ₃₅face.[46, 47] It is worth noting that it is the symmetry of the methyl group itself that is discussed in this context. The symmetry of the sample surface may be isotropic (C_∞), independent of the symmetry of functional groups within the molecules, since the molecules can be randomly oriented in the surface plane despite pos- ₄₀sessing internal symmetry. To conclude, the observation of a split r⁻ mode indicates that the molecular packing at the silica surface of the EA deposited from water is denser and more crystalline

than the packing of the molecules deposited from the Cd²⁺ containing subphase. In direct contradiction, the presence of the ₄₅stronger d⁺ mode indicates a larger number of gauche defects, associated to a more disordered and less tightly packed monolayer. To reconcile these apparently conflicting observations, it has to be assumed that the area probed by the VSF spectrometer contains a mixture of domains or areas with more or less tightly ₅₀packed molecules, so that the d⁺ signal and the non-degenerate r⁻ signals stem from different local environments. Such reconciliation is supported by the AFM image of the sample (Figure 3) that displays a partial coverage of the monolayer on the sample surface (see concluding discussion).
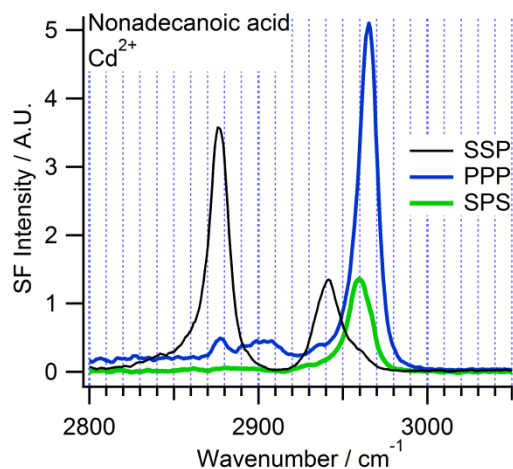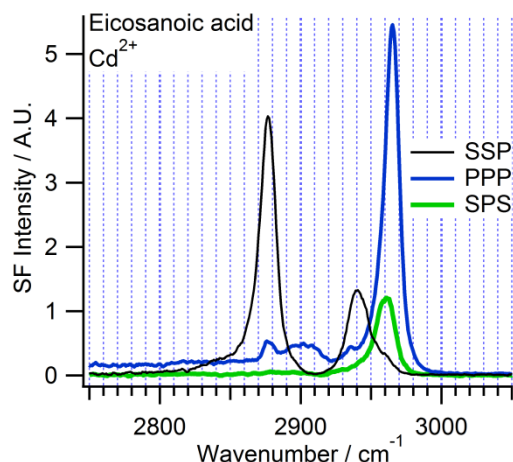
Figure 7A and B. VSF spectra of eicosanoic acid (EA) and nonadecanoic acid (NoA) both deposited on silica from a Cd²⁺ containing subphase. The spectral data show that both molecules form conformationally well or- ₆₀dered, tightly packed, monolayers with the aliphatic chains oriented approximately perpendicularly to the sample surface.

The selective replacement of hydrogen atoms with deuterium atoms offers a means to distinguish between different hydrocarbon moieties in a molecule because the CD-stretching region is ₆₅shifted approximately 800 wavenumbers away from the CH-stretching region due to isotope mass effects. In addition, the peaks appear in a different order and the r⁺_FR and r⁻ modes are sufficiently separated to enable an accurate fit of the spectra which is important to ensure a reliable orientational analysis (*vide* ₇₀*infra*). The spectra of the fully deuterated octadecanoic-D35 acid

(OA-D35, an analogue of eicosanoic acid, but with two fewer methylene groups in the chain) are shown in Figure 8. It is assumed that OA-D35 forms monolayers with properties similar to these of EA. According to the assignment based on literature sources[43, 48] the r$^-$ mode appears at 2220 cm^{-1} and the r$^+$ mode is seen at 2070 cm^{-1}. Further the d$^+$ mode is present as a small peak at ≈2100 cm^{-1} in PPP followed by the broader r$^+_{FR}$ at 2130 cm^{-1} in SSP and PPP. The ratio of the d$^-$, barely discernible at 2200 cm^{-1}, to the r$^-$ intensity is the most accurate conformational order indicator for the CD-region.[43] Because of the almost complete lack of d$^-$ signal combined with a strong r$^-$ peak we conclude that this monolayer is tightly packed, similar to the EA and NoA monolayers.
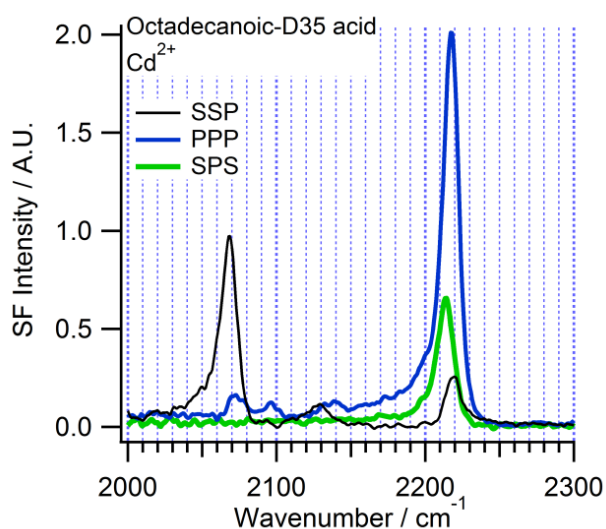
Figure 8 VSF spectra of octadecanoic-D35 acid (OA-D35) deposited on silica from a Cd^{2+} containing subphase. Note that the r$^-$ peak (at 2215 cm^{-1}) and the r$^+_{FR}$ peak (2130 cm^{-1}) do not overlap as is the case for the EA (Compare Figure 7A).

Orientation of the aliphatic chains

The average tilt of the terminal methyl group (and thus the tilt of the aliphatic chain) relative to the surface normal can be estimated based on the relative intensities of the spectral peaks in the different polarization combinations. This analysis indicates that the aliphatic chains are oriented almost perpendicular to the surface, and the findings gain further support from arguments based on the odd / even effect and isotope substitution experiments. The orientational analysis is performed by calculating the predicted intensities in different polarization combinations of the selected vibrational mode. The ratios of theses intensities are subsequently compared to the corresponding intensity ratios of the sample spectra, retrieved from fits of a model function. The theoretical foundations and limitations of the orientational analysis are thoroughly described in the literature.[21, 41, 43, 46, 49, 50] We base the analysis on the r$^-$ mode since for the type of monolayer and interface under consideration the r$^+$ signal is always strongest in SSP independent of the tilt angle, which limits the accuracy of the analysis. In addition the orientational analysis of the r$^+$ mode requires more input parameters (the Raman depolarization ratio), and the fact that the signal is indiscernible in the SPS polarization combination further increases the uncertainties. The main drawbacks with using the r$^-$ mode are i) the difficulty of accurately

fitting it in the SSP polarization combination due to overlap with the r$^+_{FR}$ mode, and ii) the dubious foundations of the assumption of C_{3v} symmetry of the methyl group.[45, 46] The fitting problem, however, can be alleviated by using a deuterated methyl group where the modes do not overlap (*vide supra*). In our analysis we assume C_{3v} symmetry of the deuterated methyl group, that the refractive index of the surface film, n', equals 1.16 (which has been shown to be a reasonable assumption[49]), C_∞ symmetry of the sample surface, and finally that the tilt angle has a δ-distribution, meaning that every molecule has the same tilt angle. Furthermore, the refractive index of air was trivially set to 1.0 and refractive indices of silica for the different frequencies were taken from the literature.[51]
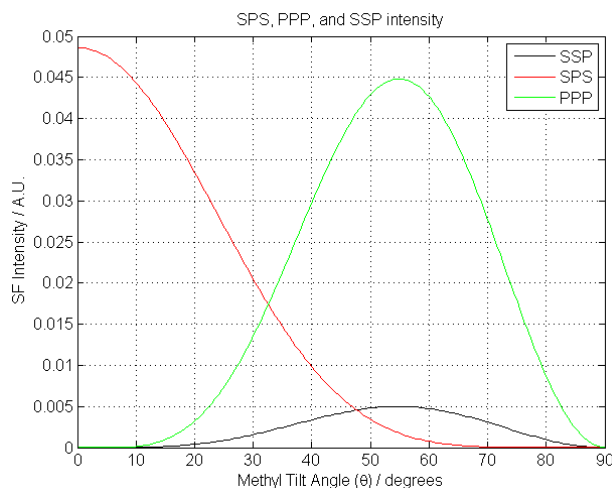
Figure 9 Calculated intensities of the antisymmetric methyl stretching vibration, r$^-$, in different polarization combinations as a function of the methyl group tilt angle relative to the surface normal. The curves are approximately similar for the CH and CD vibrations.

Figure 9 shows the calculated amplitude for the r$^-$ mode in the three polarization combinations as a function of the tilt angle, $θ$, of the methyl group's C_{3v} axis relative to the surface normal. The plot shows that this vibrational mode gives a stronger signal in SPS than in SSP at tilt angles lower than ≈48° and stronger in SPS than in PPP at tilt angles lower than approximately 30 degrees. Comparing the fitted intensities of the OA-D35 spectra to the plotted curves reveals that the tilt of the methyl group is approximately 40°. (The parameters used to fit the spectra with equation (1) are presented in the supporting information). The SSP and PPP spectra of the EA and NoA in the CH-region, which can be accurately fitted, give the same result. This indicates that the aliphatic chains are oriented approximately perpendicular to the surface, since the angle between the chain axis and the terminal methyl group is 35.5° provided the aliphatic chains have an all *trans* conformation.[52] This estimated tilt angle is also in agreement with investigations based on X-ray techniques reported in the literature.[9, 10] Additional evidence that the chains are oriented perpendicular to the surface is obtained from the fact that the spectra of EA and NoA are identical, indicating that they have the same tilt angle. Odd and even numbered chains can only display the same tilt angle for the terminal methyl group if the backbone is oriented perpendicular to the surface. Provided the fatty acid molecules are anchored to a surface and not free to rotate

around their long axis, the bonds connecting an odd numbered and an even numbered terminal methyl group would otherwise have different apparent tilt angles.[53, 54]

3.3.2. Branched chain fatty acids

19-methyl-eicosanoic acid

The VSF spectra of 19-MEA shown in Figure 10 share considerable similarities with those of EA and NoA (Figure 7). The main differences are the slightly larger intensity of the d$^+$ signal and the distinct r$^-$ signal in SSP for 19-MEA. Further, the high wavenumber side of the r$^-$ peak in SSP has a shoulder at 2980 cm^{-1}, which is also evident when trying to fit the spectrum to a model function where it causes a shift of the peak center frequency of approximately five wavenumbers. This reveals that the antisymmetric stretching mode is not fully degenerate (*vide supra*), indicating that the free rotation of the methyl groups is slightly more hindered than for the EA. This could either be due to intramolecular steric contact between the two groups, or because the methyl branch is in contact with adjacent molecules. Finally, the vibration of the methine group at the ω-1 carbon which should be located at approximately 2900 cm^{-1} is absent in the spectra of both 19-MEA and 18-MEA (Figure 12). This could partly be explained by the fact that this particular mode is very weak, and is rarely discernible in VSF spectra, and in addition the methine bond may be oriented almost parallel to the surface which would further reduce its intensity.[41]
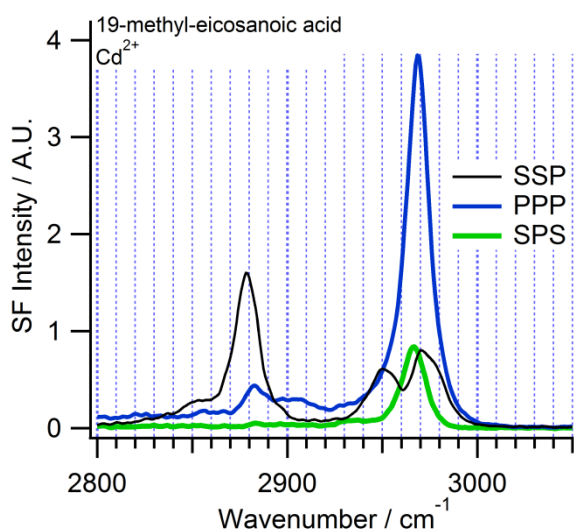
Figure 10 VSF spectra of 19-methyl-eicosanoic acid (19-MEA) deposited on silica from a Cd^{2+} containing subphase. Compared to the straight chain analogue, the stronger d$^+$ peak indicates more disordered aliphatic chains. Also note the more intense r$^-$ peak in SSP.

The more pronounced d$^+$ peak of 19-MEA is indicative of a slightly more disordered monolayer than its straight chain analogues. This is not an unexpected finding since the area per molecule is larger, and the additional methyl group is likely to prevent closer packing and consequently induces *gauche* defects. Note that *gauche* defects are not the only plausible explanation for the observation of methylene signal. It could be induced both by a shift in the vibrational frequency (for example by the inductive effect of an electron withdrawing or donating atom or functional group adjacent to the methylene group) or by the presence of a substituent that breaks the symmetry of the aliphatic chain. However, neither of these arguments apply to 19-MEA. The two terminal methyl groups are in fact indistinguishable (this also means that the molecule is non-chiral, in contrast to 18-MEA) and are thus expected to have the same vibrational frequencies; furthermore they do not break the intramolecular coupling of the methylene modes (*vide supra*). This strengthens the assertion that the observed methylene signal indeed stems from *gauche* defects in the aliphatic chains.
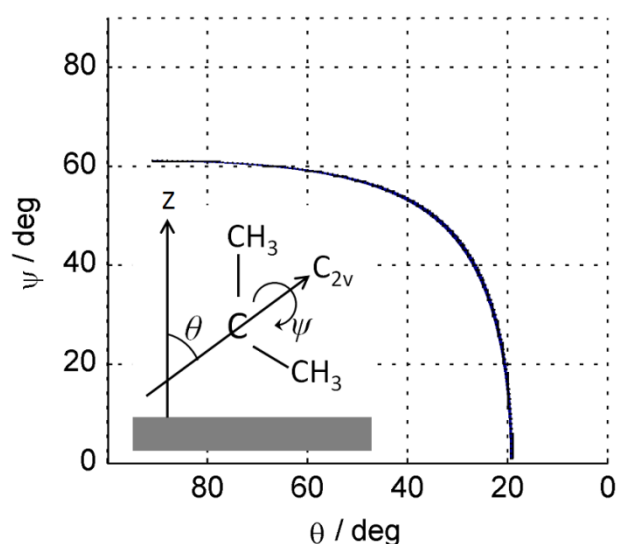
Figure 11. The set of possible tilt and twist angles of the 19-MEA dimethyl moiety and the coordinate system used to define the tilt and twist angles (Θ and ψ).

The orientational analysis of molecules containing dual methyl groups with fixed relative orientation have previously been performed for leucine[55] and 2,4-dimethylbenzene.[56, 57] To a first approximation, the orientation of the dimethyl moiety can be determined based on the calculation of spectral intensities from the combined r$^-$ modes of its two methyl groups. The required second order susceptibility tensor elements are described in the literature.[58] The tilt and twist angles (Θ and ψ) are defined according to the inset in Figure 11, where $\psi = 0$ means that the plane containing the two methyl groups is parallel to the z-axis. The angle between the C_{3v} symmetry axes of the two methyl groups, which is ≈109.5° for the sp3 hybridized carbon, appears as a constant in the equations (see the supporting information). Based on the tensor elements, the orientation of the functional group is estimated according to the same principles and assumptions as described earlier, but since the spectral intensities are a function of two variables (Θ and ψ), the resulting plots form surfaces instead of curves (Compare Figure 9 and Figure S3 in the supporting information). By dividing the spectral intensities of the different polarization combinations and plotting the values corresponding to the ratios of the measured intensities only, a set of tilt and twist angels is determined. The ratios of SPS/SSP and SPS/PPP give identical results, which are shown in Figure 11. The ratio of PPP/SSP however returns a slightly different result, which is not unexpected, since the calculated spectral intensities of these two polarization combinations differ only by constants

(i.e. the intensity surfaces in the Θ and ψ space have the same shape) which increases the sensitivity to error (See figure S3 in the supporting information). The result shows how the twist and tilt angles which are consistent with the experimental data can vary over a large range (although the set of *combined* angles is more restricted) and thus only limited conclusions can be drawn about the actual orientation of the dimethyl moiety. At higher tilt angles the SF intensity is expected to decrease substantially and thus the highest tilt angles, and their corresponding twists, can most likely be discarded from the set of possible angles, although no precise limit of this can be determined. To further constrain the range, it would be necessary to determine the absolute spectral intensity, which is not feasible with the instrumentation em-

ployed. In addition, the fit of the SSP spectrum with the model function reveals that both the in plane and out of plane antisymmetric modes are present to a certain degree, which further complicates the analysis (*vide infra*). Moreover, it must be pointed out that even if the orientation of the dimethyl moiety were completely determined it would not necessarily be possible to compute the corresponding chain tilt since the (albeit limited) gauche defects challenge the assumption of an all *trans* aliphatic chain. This is essential if the orientation of the dimethyl group is to be related to the chain tilt. A complete analysis to determine both the chain tilt and the orientation of the dimethyl group would hence require the use of a complimentary technique, such as X-ray diffraction.
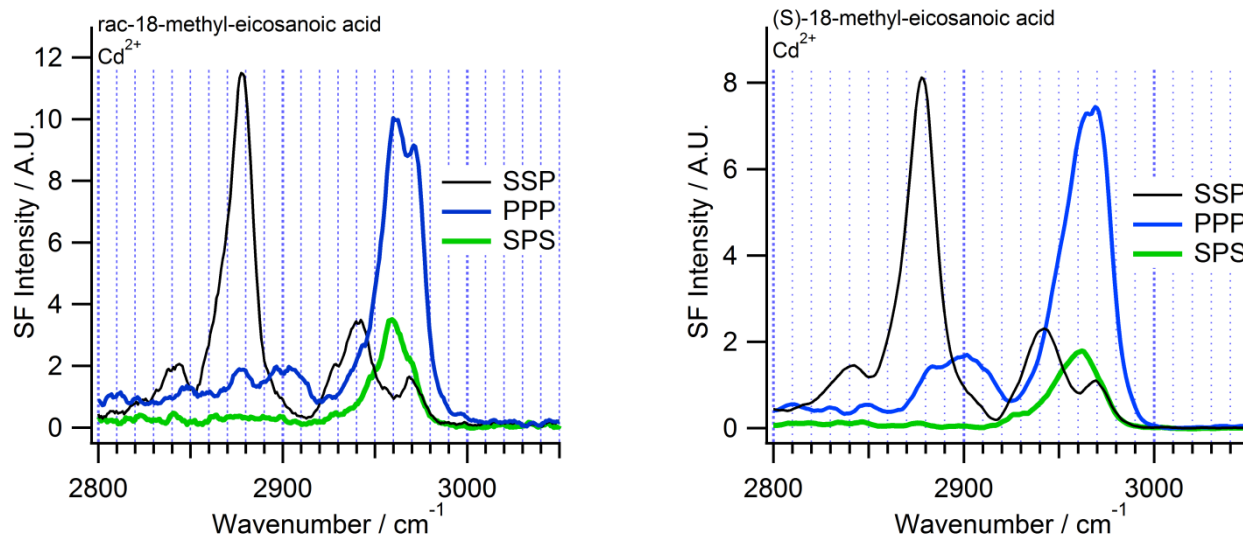
Figure 12A and B. VSF spectra of racemic 18-methyl-eicosanoic acid (rac-18-MEA) and chiral (S)-18-methyl-eicosanoic acid ((S)-18-MEA) deposited on silica from a Cd^{2+} containing subphase. The spectra of the ((S)-18-MEA) were obtained using a picosecond VSF spectrometer described elsewhere.[27]

18-methyl-eicosanoic acid

Compared to the 19-MEA and the straight chain fatty acids the spectra of the chiral and racemic 18-MEA in Figure 12, (and which are identical within the experimental error) show a slightly stronger d^+ intensity. This indicates a less well ordered monolayer, consistent with the larger area per molecule of the 18-MEA. The methylene in the ω-2 position is separated from the remaining part of the aliphatic chain by the ω-3 carbon carrying the 18-methyl group, and would thus be likely to generate a d^+ signal irrespective of the molecular conformation, provided its dipole transition moment is not parallel to the sample surface. This would in fact be the case if the aliphatic chain were in an all *trans* conformation and perpendicular to the surface.

It is evident from the spectra that the antisymmetric methyl stretch is non-degenerate and both the in plane and out of plane modes are clearly resolved in the PPP and SPS spectra. Intensity plots of the same type as shown in Figure 9 for the r^+, r^-_{ip}, and r^-_{op} of a single methyl group have been presented in an article by Bain et al.[46], but were only partly in agreement with their observed data. The general trend was that the r^+ mode is strongest in SSP followed by r^-_{ip}, and that r^-_{ip} is strongest in PPP and SPS, while r^-_{op} has a considerably lower intensity than the other modes in all three polarization combinations. However, the picture is far more complicated for the present dimethyl case, since interfer-

ence will take place between the two methyl groups.

By selective deuteration of one of the methyl groups in 18-MEA it is possible to distinguish them. Figure 13 shows spectra of the CH- and CD-stretching regions of racemic 18-methyl-D3-eicosanoic acid (rac-18-D3-MEA). The intensity of the signal from the deuterated methyl group in the 18-position is very weak, suggesting that the C_{3v}-axis of this methyl group is close to parallel to the sample surface. This claim is supported by the fact that the spectra of the CH region, now only carrying information about the 20-methyl group, are quite similar to the spectra of the rac-18-MEA in Figure 12. Although in principle it is possible to determine the tilt angle of the 20-methyl group, the difficulties associated with non-degenerate r^- vibration (vide supra) in practice preclude this.

3.4 Concluding discussion: The influence of the subphase on the Langmuir and Langmuir-Blodgett deposited monolayer properties

By combining the results obtained from the Langmuir trough, the AFM, and the VSFS spectroscopy, a more complete picture of the influence of the subphase emerges, since these techniques probe different aspects of the surfaces. While the Langmuir trough probes the macroscopic behavior of the entire monolayer, the AFM is sensitive to features on the nm scale and VSFS probes the structural average of a sub mm^2 area. The compression iso-

therm shows that in the absence of Cd^{2+} ions the EA monolayer is less condensed, and, upon deposition, the AFM images reveal that the resulting monolayer only partially covers the surface. The VSF spectrum of the deposited monolayers displays a non-degenerate antisymmetric methyl stretch, which is indicative of a very tightly packed monolayer while at the same time the stronger methylene signal indicates a conformationally disordered film with more *gauche* defects. This apparent contradiction is consistent with a non-homogeneous monolayer containing both tightly packed and disordered areas. It is likely that the disordered areas are in the vicinity of the borders between monolayer and

bare regions where the film has disintegrated during deposition. In contrast, the film deposited from the Cd^{2+} containing subphase results in full coverage of the surface with a more homogeneous, *gauche* defect free, but slightly less tightly packed monolayer (respectively indicated by the absence of methylene signal and the presence of a degenerate antisymmetric methyl stretch). This clearly shows the necessity of combining different techniques, since i) the AFM is not capable of revealing the molecular conformation within the domains and ii) the interpretation of the VSF spectra would otherwise have relied on the erroneous, but customary, assumption of a homogeneous monolayer.
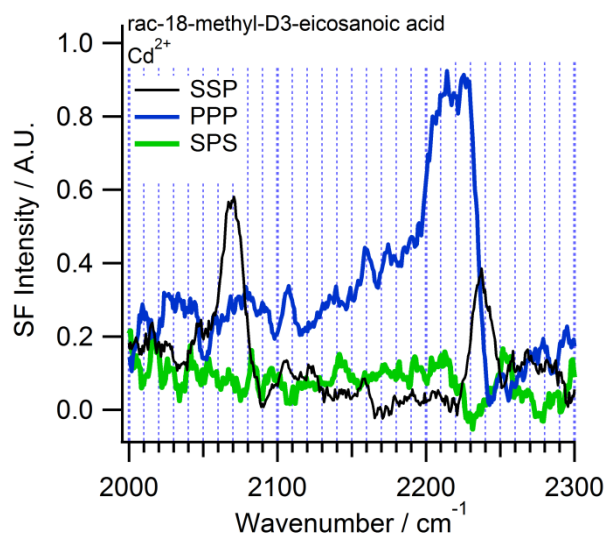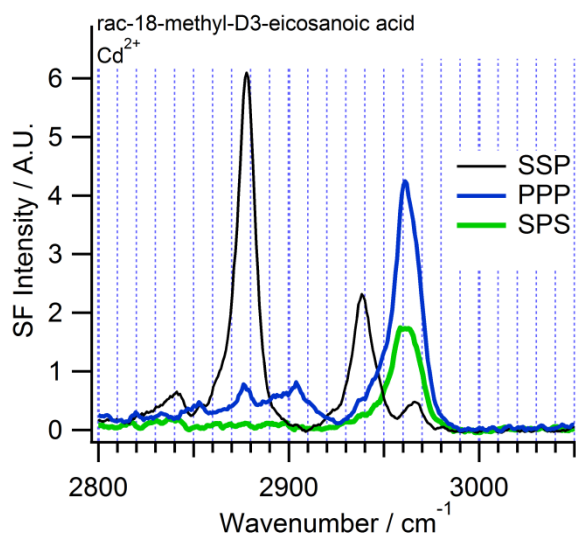
Figure 13A and B. VSF spectra showing the CH-stretching and CD-stretching regions of racemic 18-methyl-D3-eicosanoic acid (rac-18-D3-MEA) deposited on silica from a Cd^{2+} containing subphase.

3.5 Concluding discussion: Molecular structure and orientation of the straight and branched chain fatty acids

Only monolayers deposited from Cd^{2+} containing subphase were studied for the branched chain samples. Chiral molecules give rise to weak spectroscopic signals in three additional polarization combinations, but to the best of our knowledge their use for orientational analysis has not been explored.[59, 60] Attempts were made to record data in the chiral polarization combinations for (S)-18-MEA and signals with an intensity of a few percent of the non-chiral signals were detected (data not shown). Thus we conclude that with the currently available methods for data analysis there is no observable difference between the pure (S) enantiomer form and the racemic mixture of the 18-MEA indicated by *any* of the three techniques used that can provide any additional information about the structure and orientation of the monolayers. Furthermore, racemic mixtures commonly form slightly more dense crystals than the corresponding pure enantiomer,[61] but the expected difference is small ($\approx$ 1% higher density), and if this occurs for 18-MEA it is below the detection level.

All the branched chain fatty acids form nm size domains when deposited, the 19-MEA larger than the 18-MEA. Since the amount of *gauche* defects is small it can further be concluded that the domains are conformationally well ordered, and the observed methylene signal thus stems from the domain boundaries, where the aliphatic chains are expected to be slightly more disordered due to the absence of neighbouring molecules.

tension to this work would thus be to image monolayers of branched chain fatty acids deposited at varying pressure and determine whether the domain spacing and internal conformational order can be independently controlled. Despite detailed spectroscopic data, existing analysis methods are incapable of shedding light on the chain tilt and the precise molecular orientation of the two methyl groups. While the relatively small area per molecule in the floating monolayer is consistent with a small chain tilt, it can only be speculated that this structure remains upon deposition onto a solid substrate.

3.6 Concluding discussion on the domain formation

The fact that a methyl-branch causes domain formation is a remarkable observation. Similar domains have been observed before in the work of Krafft[62] and Schwartz[63] both of whom used "diblock" surfactants of hydrocarbon and fluorocarbon and both of whom deposited Langmuir Blodgett layers from self-assembled films at the water-air interface. Krafft has also directly observed such domains, or surface micelles at the liquid–air interface using synchrotron radiation.[64] In the work of Schwartz the hydrocarbon chain was terminated with a charged polar group rendering it a more traditional surfactant and the orientation of the molecules on the surface is rather unambiguous.[63] In the case of Krafft there is no polar group but the monolayer is nonetheless self-assembled into essentially two phase, 2D "micelles" with the lowest polarity fluorocarbon phase towards the air and the hydrocarbon region in contact with water and then, after deposition,

substrate.[62, 64] The aggregate size in both cases is of the order of a few thousand molecules, which is comparable to that observed here (roughly 1 500 for 18-MEA and 9 000 for 19-MEA, based on the aggregate size and the area per molecule from the LB isotherms). There is as yet no firm consensus for the discreet nature of the domains. Schwartz argues that the aggregates are essentially micelles with intrinsic curvature imposed by the mismatch between FC and HC chain packing areas and that the outer molecules of the aggregates are lying horizontally while the inner molecules stand vertically. Krafft on the other hand envisages that the domains remain independent even up to large compression due to electrostatic repulsion arising from the dipoles formed by the FC-HC interface.[65] Stabilization of domains in 2D, two phase films was first proposed by McConnell. For the case of the branched fatty acids investigated in this work there is no analogous internal boundary between incompatible phases. The additional methyl group of 18-MEA is furthermore in the horizontal plane according to the VSFS analysis. It seems therefore more likely that a curvature effect is responsible for the domains. The fact that the domains are smaller as the branch goes from the 19th to the 18th carbon is consistent with this idea (though not proof). The domains appear to have constant height and there is no evidence for edges with horizontal or even off-vertical molecules, though as argued above there is more disorder associated with the edge molecules. There is no corresponding structural information from the liquid–air interface so the following arguments are speculative, but support the idea that the domains are a feature resulting from the self-assembly prior to LB deposition.

The significant difference in the area per molecule of the branched species compared to the straight chain at the deposition pressure is evidence that the molecules have an intrinsic packing curvature. The optimum packing area for the carboxylic acid group is given by the value for EA, A_{EA}, while the area at the hydrocarbon-air interface is determined by the position of the branch and is reflected in the area per molecule. The supporting information (Section 3.) describes how an effective radius of curvature that is associated with the packing of branched molecules into aggregates can be calculated and these values are of the order of 28 and 40 nm for 18-MEA and 19-MEA respectively. It can be argued that rather than forming flat structures on the liquid–air interface the domains are in fact caused by spherical caps, on the surface where the curvature is imposed by the intrinsic packing parameter of the molecules, which in this case would be greater than 1 and impose a weak inverse micellar curvature The convex structure would cause the water surface to be lifted under the domains as depicted in Figure S6 in the supporting information. The gravitational penalty in this case is negligible compared to the surface energy terms. While the branched molecules could adopt gauche defects to permit a flat packing the resultant headgroup area would be large compared to that of EA and thus energetically unfavorable. By adopting the slight curvature the contact between water and hydrocarbon associated with the headgroups can be effectively eliminated. The gravitational penalty is negligible, but the energy penalty lies in the fact that such a spherical cap must have an exterior annulus where there is contact of the outermost hydrocarbon chains with the water surface. Simple calculations such as those shown in the supporting information indicate that the reduction in surface energy associated with the curvature is comparable to the penalty of the annulus. We speculate that the domain size is thus determined by the spherical cap height at which these terms balance, and the maximum value of the domain lateral extent is thus limited by the size of a hemispherical cap. This would correspond to the two numbers above – 28 nm and 40 nm. The ratio of these two values is highly reminiscent of the ratio of the domain sizes, and the actual size is smaller. The annulus energy penalty is maximized for a hemispherical cap (hydrocarbons lying parallel to water surface) so the expected size should be smaller as observed. When the domains are transferred to the rigid solid-air interface, the caps are forced to readapt their geometry to a flat structure and deform. Thus the AFM images reveal irregular structures of uniform height and size. This process is driven entirely by the packing properties of the molecules and furthermore indicates that chiral and racemic samples behave identically in this regard. The closer the methyl branch is to the terminal methyl group, the lower the intrinsic curvature of the molecule and larger domains are thus favored.

4. Summary and Conclusions

Any one technique is only as good as the assumptions on which it rests. VSFS is an excellent example of this, since most orientational analysis is dependent upon the assumption that the spectrum is representative of a uniform film. It is not always the case that such spectroscopic studies are backed up by other techniques. The combined approach used in this work, where the VSFS is supported by Langmuir-Blodgett trough and AFM studies, has shown to be vital for understanding both the molecular orientation and conformation, as well as the deposited monolayer morphology of the selection of straight chain, iso, and anteiso fatty acids used here. Identification of inhomogeneous monolayers, featuring for instance domain formation (in the case of branched chain fatty acids) or partial coverage of the substrate surface (on deposition of straight chain fatty acids from neat water) allowed unambiguous analysis of spectral data which would otherwise have been impossible, or at least seriously compromised by, the assumption of homogeneity.

The results underscore that the composition of the subphase is of profound importance when performing LB-depositions and also strongly influences the shape of compression isotherms. The addition of Cd^{2+} ions to the subphase induces a contraction of the floating monolayer and results in conformationally well-ordered deposited monolayers. Corresponding monolayers deposited from neat water are patchy. Their spectra thus show characteristic indications of *both* very tight packing *and* conformational disorder, which must necessarily stem from different regions. The disorder is most likely associated with the boundaries of the covered areas. The domain size is considered to be determined by the curvature of the aggregates at the liquid-air surface, in turn controlled by the branched fatty acid packing parameter. This implies a 3D surface film consisting of micelles shaped like spherical caps on the aqueous interface.

None of the three techniques applied here were capable of distinguishing between the monolayers of the chiral (S) form and racemic mixture of 18-MEA. This suggests that the differences in molecular conformation, orientation, and film morphology are minor, if present at all. An important implication of this finding is

that the racemic mixture may thus well be sufficient in model systems for investigating the properties of the boundary film in human hair. An obvious next step is to investigate the behavior of mixtures of branched and straight chain fatty acids, since in reali-
5 ty such boundary films consist of a complex mixture of fatty acids.

5. Acknowledgements

6. References

1. S. Abrahamsson, S. Ställberg-Stenhagen and E. Stenhagen, *Progress in the Chemistry of Fats and other Lipids*, 1964, **7**, 1-157.

2. L. N. Jones and D. E. Rivett, *Micron*, 1997, **28**, 469-485.

20 3. T. Kaneda, *Microbiol Rev*, 1991, **55**, 288-302.

4. H. Tanamachi, S. Tokunaga, N. Tanji, M. Oguri and S. Inoue, *J Cosmet Sci*, 2010, **61**, 147-160.

5. J. F. Liljeblad, V. Bulone, E. Tyrode, M. W. Rutland and C. M. Johnson, *Biophys. J.*, 2010, **98**, L50-52.

25 6. E. Tyrode, P. Niga, M. Johnson and M. W. Rutland, *Langmuir*, 2010, **26**, 14024–14031.

7. U. Roze, D. C. Locke and N. Vatakis, *J. Chem. Ecol.*, 1990, **16**, 725-734.

8. M. T. Madigan, J. M. Martinko and J. Parker, *Biology of
30 Microorganisms*, 10'Th International edn., Pearson Education Ltd., London, 2003.

9. A. Ulman, *Ultrathin organic films*, Academic Press Inc., San Diego, CA, USA, 1991.

10. J. B. Peng, G. T. Barnes and I. R. Gentle, *Adv. Colloid Interface Sci.*,
35 2001, **91**, 163-219.

11. B. P. Binks, *Adv. Colloid Interface Sci.*, 1991, **34**, 343-432.

12. M. Perrin, Ecole Polytechnique Federale de Lausanne, 2006.

13. H. Matuo and D. A. Cadenhead, *Colloids Surf.*, 1989, **41**, 287-301.

14. R. L. McMullen and S. P. Kelty, *J. Phys. Chem. B*, 2007, **111**, 10849-
40 10852.

15. U. Natarajan and C. Robbins, *J Cosmet Sci*, 2010, **61**, 467-477.

16. S. Breakspear, J. R. Smith and G. Luengo, *J Struct Biol*, 2005, **149**, 235-242.

17. H. Mizuno, G. S. Luengo and M. W. Rutland, *Langmuir*, 2010, **26**,
45 18909-18915.

18. D. J. Cundy and P. A. Gurr, *Org. Prep. Proced. Int.*, 2000, **32**, 461-468.

19. P. Guyot-Sionnest, J. H. Hunt and Y. R. Shen, *Phys. Rev. Lett.*, 1987, **59**, 1597-1600.

50 20. G. L. Richmond, *Chemical Reviews*, 2002, **102**, 2693-2724.

21. H. F. Wang, W. Gan, R. Lu, Y. Rao and B. H. Wu, *Int Rev Phys Chem*, 2005, **24**, 191-256.

22. X. Y. Chen, J. Wang, C. B. Kristalyn and Z. Chen, *Biophys. J.*, 2007, **93**, 866-875.

55 23. J. Liu and J. C. Conboy, *Langmuir*, 2005, **21**, 9091-9097.

24. L. F. Voss, C. M. Hadad and H. C. Allen, *J. Phys. Chem. B*, 2006, **110**, 19487-19490.

25. G. Ma and H. C. Allen, *Langmuir*, 2006, **22**, 5341-5349.

26. E. Tyrode, M. W. Rutland and C. D. Bain, *J Am Chem Soc*, 2008,
60 **130**, 17434-17445.

27. C. M. Johnson, E. Tyrode, S. Baldelli, M. W. Rutland and C. Leygraf, *J. Phys. Chem. B*, 2005, **109**, 321-328.

28. W. H. Jang, J. Drelich and J. D. Miller, *Langmuir*, 1995, **11**, 3491-3499.

65 29. J. D. Miller, K. Q. Fa, J. V. Calara and V. K. Paruchuri, *Colloid Surface A*, 2004, **238**, 91-97.

30. M. C. Fuerstenau, G. Jameson and R.-H. Yoon, eds., *Froth Flotation: A Century of Innovation*, Society of Mining, Metallurgy, and Explorationb, Inc., Littleton, Colorado, USA, 2007.

70 31. J. F. D. Liljeblad, *A Spectroscopic Study of Interfacial Films: Internal Structuring, Stability and Hydration*, Chemical Science and Engineering, KTH Royal Institute of Technology, Stockholm, 2012.

32. J. F. D. Liljeblad and E. Tyrode, *Journal of Physical Chemistry C*, 2012, **116**, 22893-22903.

75 33. D. M. Balthasar, D. A. Cadenhead, R. N. A. H. Lewis and R. N. Mcelhaney, *Langmuir*, 1988, **4**, 180-186.

34. S. Kundu and D. Langevin, *Colloid Surface A*, 2008, **325**, 81-85.

35. J. Peltonen, M. Linden, H. Fagerholm, E. Gyorvary and F. Eriksson, *Thin Solid Films*, 1994, **242**, 88-91.

80 36. R. Johann, G. Brezesinski, D. Vollhardt and H. Mohwald, *J. Phys. Chem. B*, 2001, **105**, 2957-2965.

37. S. Datta, S. Kundu and S. Hazra, *Langmuir*, 2005, **21**, 5894-5900.

38. R. A. Macphail, H. L. Strauss, R. G. Snyder and C. A. Elliger, *J Phys Chem-Us*, 1984, **88**, 334-341.

85 39. R. G. Snyder, H. L. Strauss and C. A. Elliger, *J Phys Chem-Us*, 1982, **86**, 5145-5150.

40. R. G. Snyder, S. L. Hsu and S. Krimm, *Spectrochim Acta A*, 1978, **34**, 395-406.

41. R. Lu, W. Gan, B. H. Wu, Z. Zhang, Y. Guo and H. F. Wang, *J.
90 Phys. Chem. B*, 2005, **109**, 14118-14129.

42. G. R. Bell, C. D. Bain and R. N. Ward, *J Chem Soc Faraday T*, 1996, **92**, 515-523.

43. E. Tyrode and J. Hedberg, *J. Phys. Chem. C*, 2012, **116**, 1080-1091.

44. E. Tyrode and J. F. D. Liljeblad, *Journal of Physical Chemistry C*,
95 2012, **117**, 1780-1790.

45. R. A. Macphail, R. G. Snyder and H. L. Strauss, *J Chem Phys*, 1982, **77**, 1118-1137.

46. D. A. Beattie, R. Fraenkel, S. A. Winget, A. Petersen and C. D. Bain, *J. Phys. Chem. B*, 2006, **110**, 2278-2292.

100 47. B. D. Casson, R. Braun and C. D. Bain, *Faraday Discuss*, 1996, **104**, 209-229.

48. M. R. Bunow and I. W. Levin, *Biochim Biophys Acta*, 1977, **489**, 191-206.

49. X. Zhuang, P. B. Miranda, D. Kim and Y. R. Shen, *Phys. Rev. B*,
105 1999, **59**, 12632-12640.

50. J. F. D. Liljeblad, V. Bulone, M. W. Rutland and C. M. Johnson, *Journal of Physical Chemistry C*, 2011, **115**, 10617-10629.

51. I. H. Malitson, *J. Opt. Soc. Am.*, 1965, **55**, 1205-1208.

52. J. Lobau and K. Wolfrum, *Journal of the Optical Society of America
110 B-Optical Physics*, 1997, **14**, 2505-2512.

53. N. Nishi, D. Hobara, M. Yamamoto and T. Kakiuchi, *J Chem Phys*, 2003, **118**, 1904-1911.

54. F. Tao and S. L. Bernasek, *Chemical Reviews*, 2007, **107**, 1408-1453.

55. N. Ji and Y. R. Shen, *J Chem Phys*, 2004, **120**, 7107-7112.

56. P. J. N. Kett, M. T. L. Casford and P. B. Davies, *Mol. Phys.*, 2013, **111**, 173-185.

57. P. J. N. Kett, M. T. L. Casford and P. B. Davies, *Journal of Physical Chemistry Letters*, 2012, **3**, 3276-3280.

58. S. Kataoka and P. S. Cremer, *J Am Chem Soc*, 2006, **128**, 5516-5522.

59. M. A. Belkin, T. A. Kulakov, K. H. Ernst, L. Yan and Y. R. Shen, *Phys. Rev. Lett.*, 2000, **85**, 4474-4477.

60. M. Oh-e, H. Yokoyama, S. Yorozuya, K. Akagi, M. A. Belkin and Y. R. Shen, *Phys. Rev. Lett.*, 2004, **93**, 267402.

61. C. P. Brock, W. B. Schweizer and J. D. Dunitz, *J Am Chem Soc*, 1991, **113**, 9811-9820.

62. M. P. Krafft, *Acc. Chem. Res.*, 2011, **45**, 514-524. and references therein.

63. S. M. Malone, S. Trabelsi, S. Zhang, T. R. Lee and D. K. Schwartz, *The Journal of Physical Chemistry B*, 2010, **114**, 8616-8620.

64. P. Fontaine, M. Goldmann, P. Muller, M.-C. Fauré, O. Konovalov and M. P. Krafft, *J Am Chem Soc*, 2004, **127**, 512-513.

65. A. N. Semenov, A. González-Pérez, M. P. Krafft and J.-F. Legrand, *Langmuir*, 2006, **22**, 8703-8717.